

Scale-arbitrary Invertible Image Downscaling

JINBO XING*, WENBO HU*, and TIEN-TSIN WONG[†], The Chinese University of Hong Kong, Hong Kong SAR, China

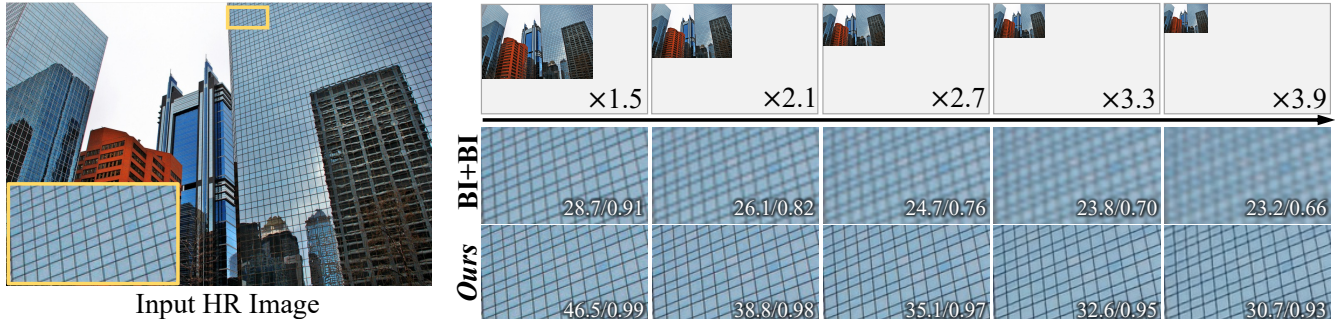


Fig. 1. Given an input high-resolution (HR) image (left) to be distributed over the Internet and required scale factors (arbitrary) to fit the target display, our method (a universal system) can downscale it to the low-resolution (LR) images (upper-right) with the HR information embedded in a nearly-imperceptible form. And whenever users want to view the details of distributed images, our method can faithfully restore the HR image with original resolution (bottom-right). A standard solution to achieve this goal is to downscale/upscale the input HR image with both Bicubic interpolation (BI+BI). We show PSNR/SSIM of restored HR image as well as the blow-up result under various scale factors.

Downscaling is indispensable when distributing high-resolution (HR) images over the Internet to fit the displays of various resolutions, while upscaling is also necessary when users want to see details of the distributed images. Recent invertible image downscaling methods jointly model these two problems and achieve significant improvements. However, they only consider fixed integer scale factors that cannot meet the requirement of conveniently fitting the displays of various resolutions in real-world applications. In this paper, we propose a Scale-Arbitrary Invertible Image Downscaling Network (AIDN), to natively downscale HR images with arbitrary scale factors for fitting various target resolutions. Meanwhile, the HR information is embedded in the downsampled low-resolution (LR) counterparts in a nearly imperceptible form such that our AIDN can also restore the original HR images solely from the LR images. The key to supporting arbitrary scale factors is our proposed Conditional Resampling Module (CRM) that conditions the downscaling/upsampling kernels and sampling locations on both scale factors and image content. Extensive experimental results demonstrate that our AIDN achieves top performance for invertible downscaling with both arbitrary integer and non-integer scale factors. Code will be released upon the publication.

CCS Concepts: • Computing methodology → Computational photography.

Additional Key Words and Phrases: Invertible image rescaling, machine learning, image reconstruction

ACM Reference Format:

Jinbo Xing, Wenbo Hu, and Tien-Tsin Wong. 2022. Scale-arbitrary Invertible Image Downscaling. *ACM Trans. Graph.* 1, 1 (January 2022), 8 pages. <https://doi.org/10.1145/nnnnnnnn.nnnnnnnn>

*Equal contribution

[†]Corresponding author

Authors' address: Jinbo Xing; Wenbo Hu; Tien-Tsin Wong, The Chinese University of Hong Kong, Hong Kong SAR, China, [jbxing, wbhu, ttwong]@cse.cuhk.edu.hk.

1 INTRODUCTION

With the rapid development of smartphone cameras, exploding amount of high-resolution images/videos are produced in our daily life. As shown in Figure 2, downscaling is necessary when distributing them over the Internet, in order to fit the displays of various resolutions. On the other hand, image upscaling/super-resolution (SR), as the inverse problem of it, is also indispensable when users want to see details of the distributed images. But the lost information during the downscaling process makes the SR problem highly ill-posed [Dong et al. 2015; Glasner et al. 2009; Yang et al. 2010]. To relieve this problem, recent works [Kim et al. 2018; Sun and Chen 2020; Xiao et al. 2020] regard the downscaling/upsampling as a dual problem and jointly optimize them. By doing so, the information from the high-resolution (HR) images can be better preserved or embedded during the downscaling process, which leads to a higher restoration performance for the upscaling counterpart.

However, existing works only consider a fixed integer scale factor, e.g., $\times 2$, $\times 3$, or $\times 4$. In real-world applications (Figure 2), we usually need to distribute images to multiple target resolutions, e.g., iPhone 13 display is 2532×1170 , iPod touch display (7th Gen.) is 1136×640 , and Apple Watch 7 display (45mm) is 484×396 , and whenever users want to view details of the distributed images, we need to upscale it. Although with certain operations (including the Bicubic interpolation [Mitchell and Netravali 1988]) on the input/output images from multiple trained scale-fixed invertible models [Sun and Chen 2020; Xiao et al. 2020], one can indirectly and virtually achieve the arbitrary scale factor, this also means numerous trained models have to be stored in place. Moreover, the experiment shows such an indirect solution cannot produce satisfactory results (Figure 3), and its performance fluctuates across the scale factors.

In this paper, we propose a *universal* encoder-decoder styled *Scale-Arbitrary Invertible Image Downscaling Network* (AIDN), to downscale/upscale images with arbitrary scale factors. The encoder

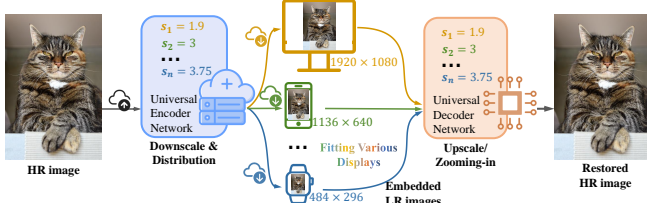


Fig. 2. Given an HR image to be distributed, our framework can universally downscale it with arbitrary scale factors to fit various target display resolutions, and whenever users want to observe details of the distributed image, our framework can faithfully restore the HR image with original resolution.

network is designed for the downscaling problem while the decoder network is for the upscaling task, and the encoder-decoder is trained jointly to address their duality. With our AIDN, the downscaling network can *natively* generate various target resolutions and embed the HR information to the LR image in a nearly imperceptible form. Simultaneously, the upscaling network can consume the embedded information to faithfully restore the original HR image, solely from the LR counterpart. The key to supporting arbitrary scale factors is our proposed *Conditional Resampling Module* (CRM). It can dynamically resample the feature map to target resolution by parameterizing the downsampling/upsampling kernels and sampling locations conditioned on both the target scale factor and the image content. The content-adaptive characteristic allows the resampling operation to adapt to the textural/structural content at both training and inference time, so that we can produce visually pleasant results. Our proposed CRM can be easily applied to multiple existing backbones in the encoder-decoder network to enable the scale-arbitrary invertible image downscaling.

We evaluated our AIDN on multiple public datasets, both quantitatively and qualitatively. Experiment results show our AIDN achieves top performance for both integer (e.g., $\times 2$, $\times 3$ and $\times 4$) and arbitrary non-integer scale factors (e.g., $\times 1.60$, $\times 2.75$ and $\times 3.20$). Moreover, the performance changes smoothly (i.e. more predictable), without fluctuation, across the scale factors, as shown in Figure 3. Also, the visualization of routing weights confirms our CRM can dynamically adjust resampling kernels for various scale factors and different image content (Section 4.5). Our contributions are summarized below.

- To the best of our knowledge, this is the first attempt to tackle the *scale-arbitrary invertible image downscaling* problem with a single encoder-decoder network. With our AIDN, not only the downscaling can conveniently fit various resolutions of the target display screens, but also the upscaling can accurately reconstruct the original HR images.
- We propose a *Conditional Resampling Module* (CRM) to dynamically resample feature maps to the target resolution according to both the required scale factor and the image content. It can be easily applied to existing SR backbones to achieve the invertible image downscaling.
- Extensive experiments demonstrate our AIDN achieves top performance for invertible downscaling with both arbitrary integer and non-integer scale factors. Moreover, the amount of parameters of our AIDN is significantly reduced ($\sim 1/10$) compared to conventional SR networks, which indicates the high efficiency of our simple yet effective system design.

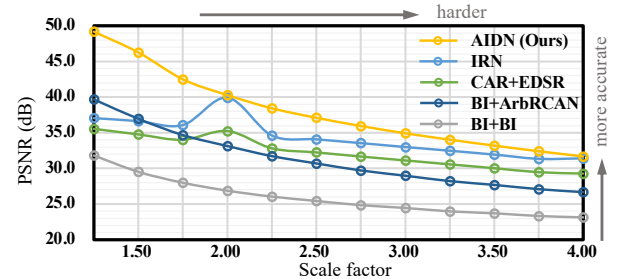


Fig. 3. Restoration quality vs. scale factor for multiple invertible image downscaling solutions, including downscaling/upsampling with both the Bicubic interpolation (BI+BI), state-of-the-art scale-arbitrary SR method (BI+ArbRCAN [Wang et al. 2021]), scale-fixed invertible image downscaling methods (CAR+EDSR [Sun and Chen 2020] and IRN [Xiao et al. 2020]), and our proposed *Scale-Arbitrary Invertible Image Downscaling Network* (AIDN), on the Urban100 [Huang et al. 2015] dataset.

2 RELATED WORK

2.1 Image Rescaling

Image downscaling and upscaling/super-resolution (SR) have been studied with a long history. Downscaling aims at reducing the resolution of images to display them on various target devices with smaller resolutions. It can be performed by resampling together with interpolation, e.g., the Bilinear and Bicubic [Mitchell and Netravali 1988] interpolation, which enjoys high efficiency but usually incurs visual artifacts, such as aliasing, ringing, blurring, etc. To tackle these problems, several detail-preserved and perceptual-quality-oriented approaches [Kopf et al. 2013; Liu et al. 2017; Oeztireli and Gross 2015; Weber et al. 2016] are proposed. On the other hand, SR tries to restore the high-resolution (HR) image from its low-resolution (LR) counterpart. Thanks to the deep learning, we have witnessed significant progress [Dai et al. 2019; Dong et al. 2014; Haris et al. 2018; Jo and Kim 2021; Kim et al. 2016; Liang et al. 2021; Niu et al. 2020; Wang et al. 2021; Zhang et al. 2018a,b; Zhong et al. 2018] on the SR problem. Recently, several works propose to learn a single network for scale-arbitrary SR, using meta-learning [Hu et al. 2019], local implicit image function [Chen et al. 2021], and scale-aware upsampling [Wang et al. 2021].

The downscaling and the upscaling act as a dual problem in nature, however, all the above works independently model them. Thus, they may be sub-optimal when working together, which is a common scenario when distributing HR images over the Internet. Differently, we model the downscaling and upscaling problems as a universal encoder-decoder network and optimize them jointly. By doing so, the downscaling and the upscaling can mutually reinforce each other to produce more visually satisfying results for both downsampled and upsampled images.

2.2 Invertible Image Conversion

The goal of invertible image conversion is to build an invertible transformation between certain visual content and an embedding image, where the original content can be restored from the embedding image whenever necessary [Cheng et al. 2021]. As a pioneer, [Xia et al. 2018] propose an auto-encoder-style network to encode the color information into the generated grayscale image, from which the original color image can be decoded back. Furthermore, several works build the invertible transformation between

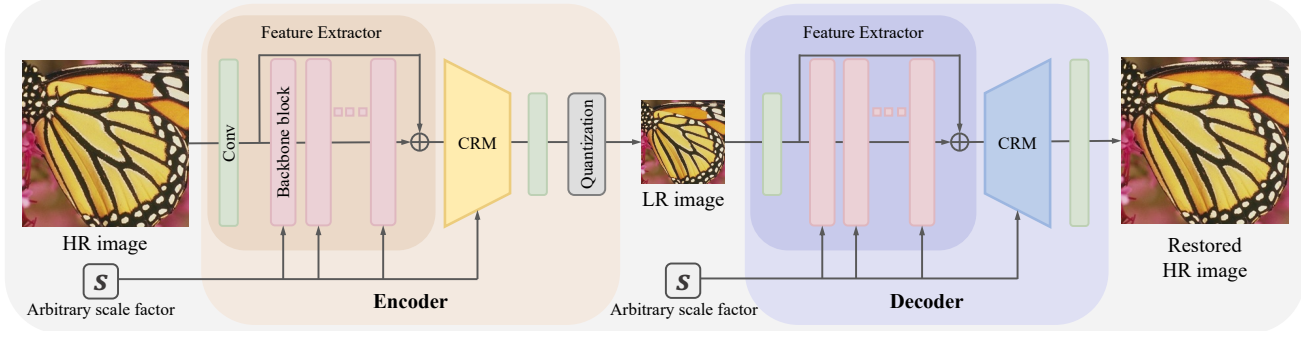


Fig. 4. Overview of the *Scale-Arbitrary Invertible Image Downscaling Network (AIDN)*. Given an HR image to be distributed and the arbitrary scale factor s , the encoder can downscale the HR image to an LR image that can fit the resolution of the target display screen; meanwhile, the decoder network can restore the original HR image solely from the LR counterpart, whenever users want to see the details of the distributed image. The CRM is our proposed conditional resampling module to resample feature maps with arbitrary scale factors.

binocular and monocular videos [Hu et al. 2020], short videos and key-frame [Zhu et al. 2020], multiview images and JPEG image [Wu et al. 2021], camera raw data and sRGB image [Xing et al. 2021]. And recently, [Cheng et al. 2021] present a generic invertible neural network (INN) [Behrmann et al. 2019; Dinh et al. 2015, 2017; Kingma and Dhariwal 2018] based framework for multiple invertible image conversion problems.

Image downscaling/upscaling can also be formulated as the invertible image conversion. [Kim et al. 2018] present a task-aware image downscaling (TAD) method to jointly optimize the downscaling and upscaling networks as a united task. [Li et al. 2018] propose to use a CNN to estimate compact-resolution images (CNN-CR), and then leverage a specified or learned SR method to restore the HR images; Recently, [Sun and Chen 2020] present a learnable image downscaling method based on content-adaptive resampler (CAR) that can be jointly trained with existing SR networks, and IRN [Xiao et al. 2020] adopts the INN to model the invertible image rescaling task as a bijective mapping from HR image to LR image while capturing the distribution of lost information using a latent variable. Although these works demonstrate the effectiveness of invertible image downscaling, they can only downscale/upscale images with fixed integer scale factors, e.g., $\times 2$ and $\times 4$. Supporting arbitrary scale factors is crucial in real-world scenarios, as shown in Figure 2. Different from the above methods, our method can downscale images with arbitrary scale factors and faithfully recover the HR images.

3 METHODOLOGY

3.1 Overview

Overall, as shown in Figure 4, our *Scale-Arbitrary Invertible Image Downscaling Network (AIDN)* contains an encoder E_θ and a decoder D_ϕ , where θ and ϕ denote their parameters, respectively. Given a high-resolution (HR) image to be distributed, I_{HR} , and the required arbitrary scale factor to fit the resolution of the target display, $s \in (1, 4]$, the encoder network E_θ can downscale the I_{HR} to produce a low-resolution (LR) image, \hat{I}_{LR} , which can be displayed on the target screen and looks like the reference LR image I_{LR} (say, the bicubic-downsampled [Mitchell and Netravali 1988] image, without loss of generality). The produced LR image \hat{I}_{LR} has the same 8-bit precision as conventional images for compatibility with current

platforms. And importantly, the decoder network D_ϕ can accurately restore the HR image \hat{I}_{HR} solely from the LR image \hat{I}_{LR} , whenever users want to see the details of the distributed image.

We design a universal encoder-decoder network for downscaling/upscaling with arbitrary scale factors to meet the requirements of conveniently fitting various resolutions of the target display in real-world applications. To leverage the duality of the downscaling and the upscaling, we train the encoder and decoder jointly with the supervision on both \hat{I}_{LR} and \hat{I}_{HR} . By doing so, the information from HR images can be embedded in the \hat{I}_{LR} and the decoder network can consume it to restore the high-quality \hat{I}_{HR} .

3.2 Network Architecture

As shown in Figure 4, the encoder and decoder sub-networks in our AIDN share a similar structure, where the encoder network contains the feature extractor, the *Conditional Resampling Module* (CRM), and the quantization layer; and decoder network consists of the feature extractor and the CRM.

Feature extractor. Considering the duality of the downscaling and the upscaling, we adopt the same architecture for feature extractors in the encoder E_θ and decoder D_ϕ networks. As EDSR [Lim et al. 2017] shows powerful capability for feature extraction in the SR task, we adopt a similar network structure for the feature extractor. For the efficiency concern, we employ the EDSR-baseline structure as the backbone block, thus, the amount of parameters of our whole network is only 3.8M, as shown in Table 1. It consists of a convolutional layer as the head and a series of residual blocks (Conv+ReLU+Conv) [He et al. 2016] as the backbone structure to learn the residual components. Note that many other types of backbone blocks are also applicable to our framework, e.g., RDN [Zhang et al. 2018b] and RCAN [Zhang et al. 2018a]. To better extract scale-adaptive features for our goal, invertible image downscaling with arbitrary scale factors, we also equip the backbone block with the scale-aware feature adaption module [Wang et al. 2021] that takes the feature map from the previous layer and the required arbitrary scale factor as input. More details about the feature extractor can be found in the *Supplementary Material*.

Conditional resampling module (CRM). After extracting features from I_{HR} or \hat{I}_{LR} , we need to resample the feature map to the target resolution with arbitrary scale factors, $s \in (1.0, 4.0]$. Previous

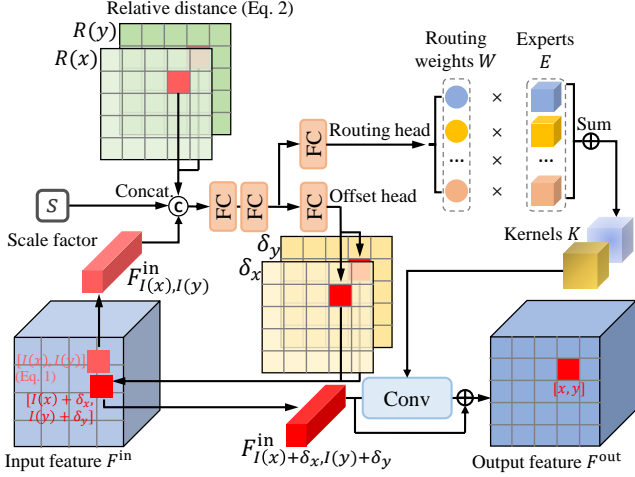


Fig. 5. Conditional Resampling Module (CRM). Given the input feature F^{in} and required arbitrary scale factor s , our CRM can dynamically resample F^{in} according to scale factor and image content, for producing the output feature F^{out} .

invertible image downscaling methods [Kim et al. 2018; Sun and Chen 2020; Xiao et al. 2020] adopt either PixelShuffle [Shi et al. 2016] or Haar transformation as the resampling module, which, however, inherently only serves a fixed integer scale factor r , i.e., $r \in \{2, 3, 4, \dots\}$ for the PixelShuffle and $r \in \{2, 4, 8, \dots\}$ for the Haar transformation.

Inspired by the conditional convolution [Chen et al. 2020; Tian et al. 2020; Yang et al. 2019; Zhang et al. 2020] that conditions convolutional kernels on instances for visual recognition, we propose a Conditional Resampling Module (CRM) to dynamically downsample/upsample feature maps to the target resolution by parameterizing the resampling kernels and sampling locations conditioned on both the required scale factor and the image content. Besides, Wang et al. [2021] also presents a scale-aware upsampling layer used for SR networks to support arbitrary scale factors. Unlike the scale-aware upsampling layer, our CRM can be used for both downscaling and upscaling, and is not only scale-aware but also content-adaptive. The content-adaptive characteristic allows our method better deal with various textural/structural patterns at both training and inference time, so that our method can produce visually satisfying results, as to be demonstrated in Sec. 4.

More concretely, as shown in Figure 5, given the input feature map F^{in} and the required arbitrary scale factor s , the goal of Conditional Resampling Module (CRM) is to produce the feature map F^{out} with the required resolution. As CRM works for downscaling and upscaling similarly, we only explain the upscaling procedure below. Taking the computation of F^{out} at coordinate $[x, y]$, $F_{x,y}^{\text{out}}$, as an example, we first project $[x, y]$ to the coordinate of F^{in} , $[I(x), I(y)]$, as:

$$I(\sigma) = \frac{\sigma + 0.5}{s} - 0.5, \quad \sigma \in \{x, y\}. \quad (1)$$

Then, we can query a feature vector of F^{in} at $[I(x), I(y)]$, $F_{I(x), I(y)}^{\text{in}}$. The feature querying can be achieved by interpolation, where we adopt the bilinear interpolation in our implementation. For each projected coordinate, we also compute a relative distance vector

$$[R(x), R(y)],$$

$$R(\sigma) = I(\sigma) - \text{floor}\left(\frac{\sigma + 0.5}{s}\right), \quad \sigma \in \{x, y\}. \quad (2)$$

Next, s , $F_{I(x), I(y)}^{\text{in}}$, and $[R(x), R(y)]$ are concatenated together and fed to two Fully-Connected (FC) layers for feature extraction and aggregation. The aggregated feature is then passed to two heads: the offset head for predicting the final sampling location offset $[\delta_x, \delta_y]$; and the routing head to predict the routing weights W for the experts E . After that, we query a new feature vector $F_{I(x)+\delta_x, I(y)+\delta_y}^{\text{in}}$ using the predicted offset $[\delta_x, \delta_y]$; and use the predicted routing weights W to combine the experts E for producing the final resampling kernels, $K = W \cdot E$. Finally, we can compute the required result $F_{x,y}^{\text{out}}$ as:

$$F_{x,y}^{\text{out}} = K * F_{I(x)+\delta_x, I(y)+\delta_y}^{\text{in}} + F_{I(x)+\delta_x, I(y)+\delta_y}^{\text{in}}, \quad (3)$$

where $*$ is the convolution operator. We can find that the kernels and sampling locations are both conditioned on the scale factor and the image content; thus, the produced output feature can be adaptive to both scale and content.

Quantization layer. The pixel value output by the convolutional layer is inherently a continuous floating-point number. But we require the downsampled image \hat{I}_{LR} to be compatible with current platforms, which should be in an 8-bit format, i.e., integers in the range of $[0, 255]$. It means we have to quantize the floating-point network-output values to 8-bit integers for producing \hat{I}_{LR} . Such operation is unfortunately not differentiable that hinders the end-to-end training of the encoder-decoder. To this end, several techniques [Ballé et al. 2016, 2017; Bengio et al. 2013; Theis et al. 2017] were proposed in the image compression field. Similarly to [Nakanishi et al. 2018], we approximate the non-differentiable round operation with a soft version:

$$\text{round}_{\text{soft}}(x) = x - \alpha \frac{\sin(2\pi x)}{2\pi}, \quad (4)$$

where α is set to 0.5 in our experiments. The quantization layer adopts the conventional $\text{round}()$ function and the gradient of Equation 4 in the forward and backward passes, respectively.

3.3 Loss Function

Following Xiao et al. [2020], we adopt two loss terms to drive the network training:

$$\mathcal{L}_G(\theta) = \mathbb{E}_{I_{\text{HR}} \in \mathcal{I}} \{ \|f(I_{\text{HR}}) - \hat{I}_{\text{LR}}\|_2^2 \} \quad (5)$$

$$\mathcal{L}_I(\theta, \phi) = \mathbb{E}_{I_{\text{HR}} \in \mathcal{I}} \{ \|I_{\text{HR}} - \hat{I}_{\text{HR}}\|_1 \}, \quad (6)$$

where the *guidance loss* $\mathcal{L}_G(\theta)$ is to supervise the produced downsampled image \hat{I}_{LR} to be similar with the conventional LR image that is generated by the Bicubic interpolation $f(\cdot)$ from the original HR image I_{HR} ; and the *invertibility loss* $\mathcal{L}_I(\theta, \phi)$ is to constrain the reconstructed HR image \hat{I}_{HR} to match I_{HR} . Here \mathbb{E} denotes the average operator over all images in training dataset \mathcal{I} ; θ and ϕ denote the parameters of encoder and decoder, respectively. Note that $\mathcal{L}_I(\theta, \phi)$ effectively imposes constraints over the parameters of both the encoder and decoder, since they are jointly trained. Altogether, we optimize the proposed AIDN by minimizing the *total loss* $\mathcal{L}(\theta, \phi)$,

$$\mathcal{L}(\theta, \phi) = \lambda \mathcal{L}_G(\theta) + \mathcal{L}_I(\theta, \phi), \quad (7)$$

Table 1. Quantitative results (PSNR) of the reconstructed HR images produced by multiple methods with various scale factors on the five benchmark datasets. Methods marked with ^{*}, [†], and [‡] are the type I, II, and III methods explained in Sec. 4.2, respectively. The **best** and second-best results are marked in bold and underline, respectively.

Method Downscaling+Upscaling	Param. (M)	Set5		Set14		B100		Urban100		DIV2K	
		$\times 2$	$\times 1.6$	$\times 2$	$\times 1.65$	$\times 2$	$\times 1.4$	$\times 2$	$\times 1.95$	$\times 2$	$\times 1.7$
Bicubic + Bicubic	-	33.66	36.10	30.24	31.83	29.56	32.95	26.88	27.05	31.01	32.46
Bicubic + EDSR- $\times 2$ [Lim et al. 2017] [*]	40.7	38.19	40.39	33.95	35.95	32.36	36.79	32.95	32.69	35.03	36.95
Bicubic + ArbEDSR[Wang et al. 2021] [†]	39.2	38.19	40.64	34.05	36.22	32.37	36.92	33.02	33.30	-	-
TAD + TAU($\times 2$)[Kim et al. 2018] [‡]	-	38.46	-	35.52	-	36.68	-	35.03	-	39.01	-
CNN-CR + CNN-SR($\times 2$)[Li et al. 2018] [‡]	-	38.88	-	35.40	-	33.92	-	33.68	-	-	-
CAR + EDSR($\times 2$)[Sun and Chen 2020] [‡]	51.1	38.94	40.09	35.61	36.45	33.83	36.41	35.24	33.28	38.26	34.29
IRN- $\times 2$ [Xiao et al. 2020] [‡]	1.7	43.99	43.42	40.79	39.24	41.32	39.63	39.92	35.28	44.32	42.00
AIDN (Ours)	<u>3.8</u>	44.13	48.81	40.81	44.25	<u>40.72</u>	52.11	40.28	39.27	<u>44.12</u>	47.49
		$\times 3$	$\times 2.75$	$\times 3$	$\times 2.8$	$\times 3$	$\times 2.2$	$\times 3$	$\times 2.35$	$\times 3$	$\times 2.55$
Bicubic + Bicubic	-	30.39	31.06	27.55	27.84	27.21	28.88	24.46	25.72	28.22	29.27
Bicubic + EDSR- $\times 3$ [Lim et al. 2017] [*]	40.7	34.68	35.35	30.53	30.90	29.27	31.38	28.82	30.91	31.26	32.69
Bicubic + ArbEDSR[Wang et al. 2021] [†]	39.2	34.73	35.34	30.61	31.04	29.30	31.46	28.90	31.11	-	-
CNN-CR + CNN-SR($\times 3$)[Li et al. 2018] [‡]	-	35.13	-	31.33	-	30.26	-	28.81	-	-	-
CAR + EDSR($\times 4$)[Sun and Chen 2020] [‡]	51.1	36.13	36.69	32.52	33.04	31.29	33.56	31.12	32.59	34.15	35.84
IRN- $\times 4$ [Xiao et al. 2020] [‡]	<u>4.4</u>	38.41	39.10	<u>35.02</u>	<u>35.60</u>	34.03	36.79	33.00	34.41	37.43	38.84
AIDN (Ours)	3.8	38.70	39.64	35.52	36.23	34.32	38.68	34.93	37.86	37.96	40.03
		$\times 4$	$\times 3.1$	$\times 4$	$\times 3.2$	$\times 4$	$\times 3.55$	$\times 4$	$\times 3.7$	$\times 4$	$\times 3.65$
Bicubic + Bicubic	-	28.42	29.89	26.00	26.98	25.96	26.32	23.14	23.38	26.66	27.10
Bicubic + EDSR- $\times 4$ [Lim et al. 2017] [*]	40.7	32.47	34.25	28.81	29.95	27.73	28.25	26.65	27.06	29.25	29.92
Bicubic + ArbEDSR[Wang et al. 2021] [†]	39.2	32.51	34.48	28.83	30.07	27.74	28.30	26.62	27.12	-	-
TAD + TAU($\times 4$)[Kim et al. 2018] [‡]	-	31.81	-	28.63	-	28.51	-	26.63	-	31.16	-
CAR + EDSR($\times 4$)[Sun and Chen 2020] [‡]	51.1	33.88	35.96	30.31	32.06	29.15	30.18	29.28	29.59	32.82	33.20
IRN- $\times 4$ [Xiao et al. 2020] [‡]	<u>4.4</u>	36.19	38.23	32.67	34.50	31.64	32.56	<u>31.41</u>	<u>31.48</u>	35.07	<u>35.71</u>
AIDN (Ours)	3.8	<u>36.06</u>	38.38	<u>32.57</u>	34.85	<u>31.50</u>	32.58	31.68	<u>32.57</u>	<u>34.94</u>	35.85

where λ is a weight for balancing the two terms and set to be 1.0 in our experiments.

4 EXPERIMENTS

4.1 Dataset and Settings

We employed the DIV2K dataset [Agustsson and Timofte 2017] to train our model, which contains 900 high-quality 2K resolution images. We followed the official training and validation set splits. Besides, we evaluated our AIDN on additional four benchmark datasets, i.e., Set5 [Bevilacqua et al. 2012], Set14 [Zeyde et al. 2010], B100 [Martin et al. 2001] and Urban100 [Huang et al. 2015].

During training, we adopted scale factors varying from 1.0 to 4.0 with a stride of 0.1, i.e., $\mathcal{S} = \{1.1, 1.2, \dots, 4\}$. To address the varying difficulties of different scale factors, we randomly sampled s with probability of $\frac{s^2}{\sum_s s^2}$ from \mathcal{S} . We leave other training details in the *Supplementary Material*, due to the space constraint.

4.2 Evaluation on Reconstructed HR Images

First, we evaluated the quality of the reconstructed HR images \hat{I}_{HR} for our AIDN and compared it with three types of state-of-the-art solutions, including:

- downscaling by the Bicubic interpolation and upscaling by the scale-fixed SR methods, i.e., Bicubic+EDSR- $\times 2/\times 3/\times 4$ [Lim

- et al. 2017], and further bicubic-downscaling the output to the target resolution with required non-integer scale factors;
- downscaling by the Bicubic interpolation and upscaling by the scale-arbitrary SR method, i.e., Bicubic+ArbEDSR [Wang et al. 2021]; and
- scaled-fixed invertible image downscaling models, i.e., TAD+TAU [Kim et al. 2018], CNN-CR+CNN-SR [Li et al. 2018], CAR+EDSR [Sun and Chen 2020] and IRN [Xiao et al. 2020].

To make the type III methods support non-integer scale factors s , we first bicubically upscale I_{HR} by $\frac{2}{s}$ or $\frac{4}{s}$ times for $1.0 < s < 2.0$ and $2.0 < s < 4.0$, respectively; and then feed it to the corresponding $\times 2/\times 4$ invertible downscaling models; finally bicubically downscale the output image to the target resolution with scale factor $\frac{s}{2}$ or $\frac{s}{4}$. Note that, this solution is not memory- and computation-efficient since it increases the resolution of images before feeding into the network and decreases the resolution after getting the network’s output. Differently, our AIDN can natively support arbitrary scale factors, without any pre- or post-processing.

Quantitative results. Table 1 shows the PSNR of reconstructed HR images \hat{I}_{HR} produced by multiple methods with various scale factors on five benchmark datasets. Our AIDN significantly outperforms the type I and II methods, which confirms that jointly modeling the downscaling and upscaling process is beneficial. For the type

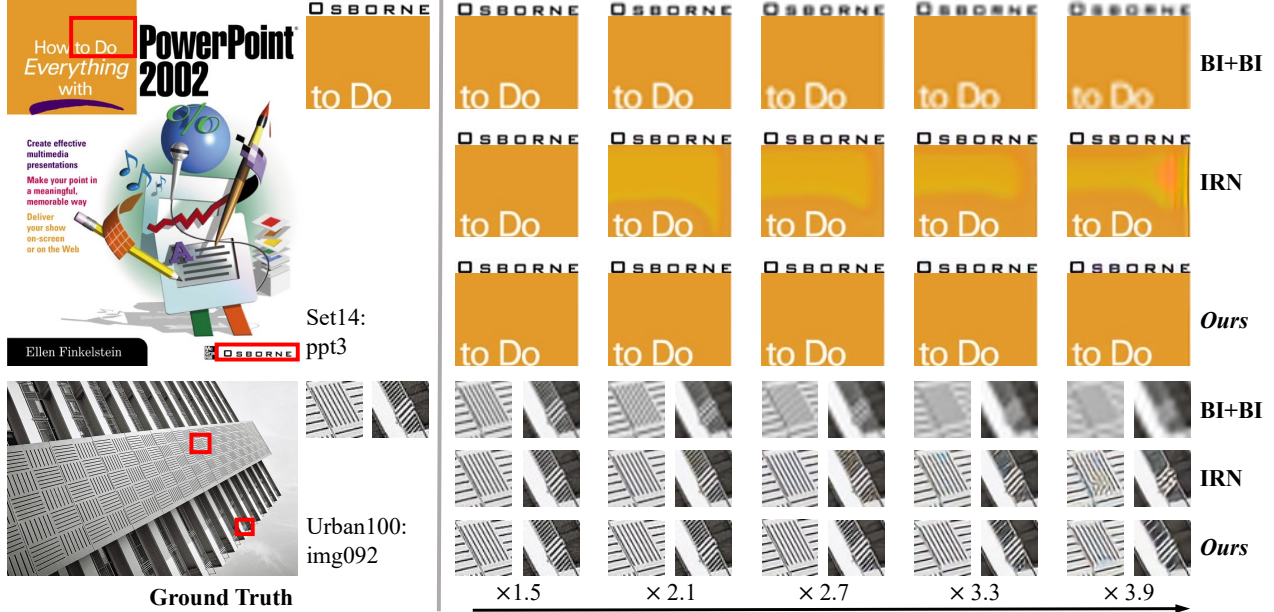


Fig. 6. Visual comparisons of the reconstructed HR images produced by the Bicubic interpolation (BI+BI), IRN [Xiao et al. 2020], and our AIDN with various non-integer scale factors (from $\times 1.5$ to $\times 3.9$). The test images are sampled from the Set14 [Zeyde et al. 2010] and Urban100 [Huang et al. 2015] datasets.

III methods that jointly optimize the downscaling and upscaling, our AIDN still outperforms them by a large margin for non-integer scale factors on all the five benchmark datasets, while achieving comparable results for integer scale factors. Note that, results of the type III methods for different scale factors are produced by multiple trained models, e.g., IRN- $\times 2$ and IRN- $\times 4$, while results of our AIDN are generated by a universal model. More importantly, as shown in Figure 3, the performance of our AIDN changes much more smoothly across scale factors, compared with the type III methods. This demonstrates the effectiveness of our CRM for invertible image downscaling with arbitrary scale factors. Besides, the number of parameters of our AIDN is very small compared with other methods, which indicates the efficiency.

Qualitative results. To further qualitatively evaluate the reconstructed HR images \hat{I}_{HR} for non-integer scale factors, we compared our AIDN with the conventional Bicubic interpolation (BI+BI) and state-of-the-art scale-fixed invertible downscaling method, IRN [Xiao et al. 2020], in Figure 6. Although the results of IRN were produced by multiple models, we can see results of our AIDN still have better perceptual quality and fewer artifacts, e.g., our method faithfully recovers both the letters and the flat region in the ‘ppt3’ case, while BI+BI suffers from blurriness for the letters and IRN incurs color distortion in the flat region; and in the ‘img092’ case, our method produces more accurate structure patterns than both BI+BI and IRN. The high fidelity of our results for various scale factors demonstrates the success of information embedding and the CRM.

4.3 Evaluation on Downscaled LR Images

Then, we evaluated the quality of downsampled LR images \hat{I}_{LR} , by measuring the SSIM between them and bicubic-downsampled images. And we compared the results of IRN and our AIDN in Table 2, we can see both of them have extremely high SSIM values. Besides, the qualitative comparison in Figure 7 shows the perceptual quality of

Table 2. SSIM between the bicubic-downscaled images and the results produced by IRN and our AIDN on the B100 [Martin et al. 2001] dataset.

Method	$\times 1.6$	$\times 2.1$	$\times 2.6$	$\times 3.1$	$\times 3.6$	$\times 3.9$
IRN	0.9963	0.9949	0.9942	0.9936	0.9932	0.9930
Ours	0.9951	0.9937	0.9924	0.9915	0.9909	0.9907

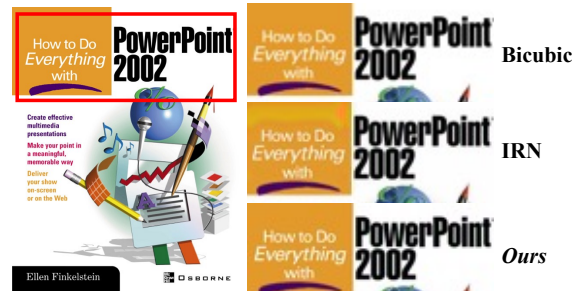


Fig. 7. Visual comparisons of the downsampled image \hat{I}_{LR} for the ‘ppt3’ image in the Set14 [Zeyde et al. 2010] with the scale factor of $\times 3.9$.

our results is even better than IRN, i.e., IRN incurs color distortion in the flat region while the result of our AIDN is free of the distortion. It indicates our downsampled images are almost the same as the conventional bicubic-downsampled ones.

4.4 Ablation Study

To verify the effectiveness of some key designs in our AIDN, we conducted ablation experiments on the Set5 [Bevilacqua et al. 2012] dataset by considering the following methods:

- **Bicubic:** down-/up-scaling with the Bicubic interpolation;
- **AIDN_{w/o CRM}:** the scale-fixed variant of our AIDN by removing the scale-aware feature adaption module in the feature extractor and replacing the CRM with the PixelShuffle;

Table 3. PSNR/SSIM results of the reconstructed HR images produced by the Bicubic interpolation, the variants of our method, and our full method on the Set5 [Bevilacqua et al. 2012] dataset. The **best** and second-best results are marked in bold and underline, respectively.

Method	$\times 2$	$\times 2.3$	$\times 2.6$	$\times 3$	$\times 3.3$	$\times 3.6$	$\times 4$
Bicubic	33.66/0.9299	32.43/0.9121	31.46/0.8944	30.39/0.8692	29.62/0.8491	29.03/0.8333	28.42/0.8104
AIDN _{w/o} CRM	45.73/0.9921	40.25/0.9766	39.33/0.9708	<u>38.62/0.9642</u>	36.86/0.9515	36.20/0.9456	35.53/0.9381
AIDN _{w/o} content	44.06/0.9866	<u>41.81/0.9794</u>	<u>40.25/0.9727</u>	<u>38.62/0.9639</u>	<u>37.68/0.9573</u>	<u>36.85/0.9513</u>	35.93/0.9429
AIDN (full method)	<u>44.13/0.9868</u>	41.86/0.9797	40.31/0.9729	<u>38.70/0.9640</u>	<u>37.79/0.9579</u>	<u>36.98/0.9516</u>	<u>36.06/0.9436</u>

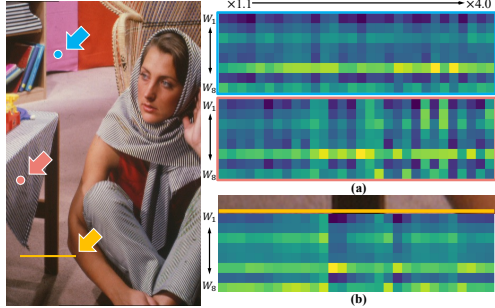


Fig. 8. Visualization of the routing weights produced by the CRM in the decoder with varying scale factors (a), and image contents (b). The blue and red dots indicate two sampling locations for fixing the image content while varying the scale factor. The yellow line is the sampling locations for fixing the scale factor to be $\times 4$ while changing the image content.

- **AIDN_{w/o} content**: the variant of our AIDN that is not content-adaptive by making the CRM only conditioned on scale factors; and
- **AIDN**: our full method.

As shown in Table 3, the PSNR/SSIM values of the Bicubic method are much lower than others, which confirms jointly modeling the downscaling and the upscaling can significantly improve the performance. Comparing the results of AIDN_{w/o} CRM and AIDN_{w/o} content, we can see the AIDN_{w/o} content performs better for the non-integer scale factors while the AIDN_{w/o} CRM performs slightly better for the integer factors. Note that, the AIDN_{w/o} CRM is designed for fixed integer scale factors, so we adopt a similar solution as the type III methods explained in Sec. 4.2 to support non-integer scale factors, which means multiple trained models have to be stored in place. Most importantly, our full method outperforms the AIDN_{w/o} content for both integer and non-integer scale factors. It demonstrates applicability of our framework and the effectiveness of our content-adaptive design for the conditional resampling module (CRM).

4.5 Discussion

Visualization of Routing Weights. To verify the effectiveness of the CRM for dynamically producing resampling kernels for different scale factors and image contents, we visualized the routing weights produced by the CRM in the decoder network, with various scale factors and image contents. We first fixed the image content and changed the scale factors to see the resulting routing weights in the decoder. As shown in Figure 8 (a), for the same location on the image, eight experts are activated differently when the scale factor varies, and the tendency to change is not the same for different locations e.g., the two marked locations with blue and red dots. Then, we fixed the scale factor to be $\times 4$ and uniformly sample the locations on a line in the image (Figure 8 (b)) to observe the resulting routing weights. We can see the eight routing weights are almost the same within the flat region, while changing sharply along with the edge in the

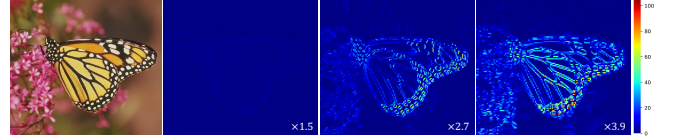


Fig. 9. Difference maps between our embedded LR images and bicubic-downscaled ones under various scale factors. We show the original HR image on the left for reference.

image. It demonstrates our CRM can produce adaptive resampling kernels according to both the scale factor and the image content.

HR Information Embedding. To further explore the embedding mechanism of HR information in the LR image, we visualized the difference maps between our embedded LR images and bicubic-downscaled ones under various scale factors in Figure 9. For convenience, we resized difference maps into the same resolution. We can observe that the differences are trivial when the scale factor is near to one, while the differences are concentrated on the edges when the scale factor is faraway from one, and the differences become more significant with the scale factors increasing. This is because there is very little HR information need to be embedded when the scale factor is near to one, while more HR information is demanded to be embedded when the scale factor increases.

Limitation. Since our AIDN encodes the HR information into the downsampled LR image, the quality of the restored HR image highly depends on the embedded information. Therefore, the downsampled LR image by our AIDN may not be resistant to general image manipulations, such as JPEG compression and editing. But many studies [Du et al. 2021; Hu et al. 2020; Liu et al. 2021; Wu et al. 2021; Xing et al. 2021] have shown that incorporating the compression during training can significantly boost the robustness to compression, which is the potential direction of our future work.

5 CONCLUSION

We present a scale-arbitrary invertible image downscaling network (AIDN) to natively downscale high-resolution (HR) images with arbitrary scale factors to fit the target displays of various resolutions for the best visual experience, when distributing HR images over the Internet. Meanwhile, the HR information is embedded in the downsampled low-resolution (LR) counterparts; thus, our AIDN can also restore the original HR images with high-quality solely from the LR images, whenever users want to see the details of the distributed images. Our technical contribution is the proposed Conditional Resampling Module (CRM) that can dynamically resample feature maps to the target resolution according to both the scale factor and the image content. Extensive ablation experiments and the visualization of the routing weights verified our design intent for the CRM. Both quantitative and qualitative results demonstrate our AIDN achieves top performance for invertible image downscaling with both arbitrary integer and non-integer scale factors.

REFERENCES

Eirikur Agustsson and Radu Timofte. 2017. Ntire 2017 challenge on single image super-resolution: Dataset and study. In *IEEE/CVF Conference on Computer Vision and Pattern Recognition Workshop (CVPRW)*.

Johannes Ballé, Valero Laparra, and Eero P Simoncelli. 2016. End-to-end optimization of nonlinear transform codes for perceptual quality. In *Picture Coding Symposium (PCS)*.

Johannes Ballé, Valero Laparra, and Eero P Simoncelli. 2017. End-to-end optimized image compression. In *International Conference on Learning Representations (ICLR)*.

Jens Behrmann, Will Grathwohl, Ricky TQ Chen, David Duvenaud, and Jörn-Henrik Jacobsen. 2019. Invertible residual networks. In *International Conference on Machine Learning (ICML)*.

Yoshua Bengio, Nicholas Léonard, and Aaron Courville. 2013. Estimating or propagating gradients through stochastic neurons for conditional computation. *arXiv preprint arXiv:1308.3432* (2013).

Marco Bevilacqua, Aline Roumy, Christine Guillemot, and Marie Line Alberi-Morel. 2012. Low-complexity single-image super-resolution based on nonnegative neighbor embedding. In *British Machine Vision Conference (BMVC)*.

Yinpeng Chen, Xiyang Dai, Mengchen Liu, Dongdong Chen, Lu Yuan, and Zicheng Liu. 2020. Dynamic convolution: Attention over convolution kernels. In *IEEE/CVF Conference on Computer Vision and Pattern Recognition (CVPR)*.

Yinbo Chen, Sifei Liu, and Xiaolong Wang. 2021. Learning continuous image representation with local implicit image function. In *IEEE/CVF Conference on Computer Vision and Pattern Recognition (CVPR)*.

Ka Leong Cheng, Yueqi Xie, and Qifeng Chen. 2021. IICNet: A Generic Framework for Reversible Image Conversion. In *IEEE/CVF International Conference on Computer Vision (ICCV)*.

Tao Dai, Jianrui Cai, Yongbing Zhang, Shu-Tao Xia, and Lei Zhang. 2019. Second-order attention network for single image super-resolution. In *IEEE/CVF Conference on Computer Vision and Pattern Recognition (CVPR)*.

Laurent Dinh, David Krueger, and Yoshua Bengio. 2015. NICE: Non-linear independent components estimation. In *International Conference on Learning Representations Workshop (ICLRW)*.

Laurent Dinh, Jascha Sohl-Dickstein, and Samy Bengio. 2017. Density estimation using real nvp. In *International Conference on Learning Representations (ICLR)*.

Chao Dong, Chen Change Loy, Kaiming He, and Xiaoou Tang. 2014. Learning a deep convolutional network for image super-resolution. In *European Conference on Computer Vision (ECCV)*.

Chao Dong, Chen Change Loy, Kaiming He, and Xiaoou Tang. 2015. Image super-resolution using deep convolutional networks. *IEEE Transactions on Pattern Analysis and Machine Intelligence (PAMI)* 38, 2 (2015), 295–307.

Yong Du, Yangyang Xu, Taizhong Ye, Qiang Wen, Chufeng Xiao, Junyu Dong, Guoqiang Han, and Shengfeng He. 2021. Invertible grayscale with sparsity enforcing priors. *ACM Transactions on Multimedia Computing, Communications, and Applications (TOMM)* 17, 3 (2021), 1–17.

Daniel Glasner, Shai Bagon, and Michal Irani. 2009. Super-resolution from a single image. In *IEEE/CVF International Conference on Computer Vision (ICCV)*.

Muhammad Haris, Gregory Shakhnarovich, and Norimichi Ukita. 2018. Deep back-projection networks for super-resolution. In *IEEE/CVF Conference on Computer Vision and Pattern Recognition (CVPR)*.

Kaiming He, Xiangyu Zhang, Shaoqing Ren, and Jian Sun. 2016. Deep residual learning for image recognition. In *IEEE/CVF Conference on Computer Vision and Pattern Recognition (CVPR)*.

Wenbo Hu, Menghan Xia, Chi-Wing Fu, and Tien-Tsin Wong. 2020. Mononizing binocular videos. *ACM Transactions on Graphics (TOG)* 39, 6 (2020), 1–16.

Xuecai Hu, Haoyuan Mu, Xiangyu Zhang, Zilei Wang, Tieniu Tan, and Jian Sun. 2019. Meta-SR: A magnification-arbitrary network for super-resolution. In *IEEE/CVF Conference on Computer Vision and Pattern Recognition (CVPR)*.

Jia-Bin Huang, Abhishek Singh, and Narendra Ahuja. 2015. Single image super-resolution from transformed self-exemplars. In *IEEE/CVF Conference on Computer Vision and Pattern Recognition (CVPR)*.

Younghyun Jo and Seon Joo Kim. 2021. Practical Single-Image Super-Resolution Using Look-Up Table. In *IEEE/CVF Conference on Computer Vision and Pattern Recognition (CVPR)*.

Heewon Kim, Myungsuk Choi, Bee Lim, and Kyoung Mu Lee. 2018. Task-aware image downscaling. In *European Conference on Computer Vision (ECCV)*.

Jiwon Kim, Jung Kwon Lee, and Kyoung Mu Lee. 2016. Accurate image super-resolution using very deep convolutional networks. In *IEEE/CVF Conference on Computer Vision and Pattern Recognition (CVPR)*.

Diederik P Kingma and Prafulla Dhariwal. 2018. Glow: generative flow with invertible 1×1 convolutions. In *Conference on Neural Information Processing Systems (NeurIPS)*.

Johannes Kopf, Ariel Shamir, and Pieter Peers. 2013. Content-adaptive image downscaling. *ACM Transactions on Graphics (TOG)* 32, 6 (2013), 1–8.

Yue Li, Dong Liu, Houqiang Li, Li Li, Zhu Li, and Feng Wu. 2018. Learning a convolutional neural network for image compact-resolution. *IEEE Transactions on Image Processing (TIP)* 28, 3 (2018), 1092–1107.

Jingyun Liang, Jiezhang Cao, Guolei Sun, Kai Zhang, Luc Van Gool, and Radu Timofte. 2021. SwinIR: Image restoration using swin transformer. In *IEEE/CVF International Conference on Computer Vision Workshop (ICCVW)*.

Bee Lim, Sanghyun Son, Heewon Kim, Seungjun Nah, and Kyoung Mu Lee. 2017. Enhanced deep residual networks for single image super-resolution. In *IEEE/CVF Conference on Computer Vision and Pattern Recognition Workshop (CVPRW)*.

Junjie Liu, Shengfeng He, and Rynson WH Lau. 2017. L0-regularized image downscaling. *IEEE Transactions on Image Processing (TIP)* 27, 3 (2017), 1076–1085.

Kunlin Liu, Dongdong Chen, Jing Liao, Weiming Zhang, Hang Zhou, Jie Zhang, Wenbo Zhou, and Nenghai Yu. 2021. JPEG Robust Invertible Grayscale. *IEEE Transactions on Visualization and Computer Graphics (TVCG)* (2021).

David Martin, Charless Fowlkes, Doron Tal, and Jitendra Malik. 2001. A database of human segmented natural images and its application to evaluating segmentation algorithms and measuring ecological statistics. In *IEEE/CVF International Conference on Computer Vision (ICCV)*.

Don P Mitchell and Arun N Netravali. 1988. Reconstruction filters in computer-graphics. *ACM Siggraph Computer Graphics* 22, 4 (1988), 221–228.

Ken M Nakanishi, Shin-ichi Maeda, Takeru Miyato, and Daisuke Okanohara. 2018. Neural multi-scale image compression. In *Asian Conference on Computer Vision (ACCV)*.

Ben Niu, Weilei Wen, Wensi Ren, Xiangde Zhang, Lianping Yang, Shuzhen Wang, Kaihao Zhang, Xiaochun Cao, and Haifeng Shen. 2020. Single image super-resolution via a holistic attention network. In *European Conference on Computer Vision (ECCV)*.

A Cengiz Oztireli and Markus Gross. 2015. Perceptually based downscaling of images. *ACM Transactions on Graphics (TOG)* 34, 4 (2015), 1–10.

Wenzhe Shi, Jose Caballero, Ferenc Huszár, Johannes Totz, Andrew P Aitken, Rob Bishop, Daniel Rueckert, and Zehan Wang. 2016. Real-time single image and video super-resolution using an efficient sub-pixel convolutional neural network. In *IEEE/CVF Conference on Computer Vision and Pattern Recognition (CVPR)*.

Wanjie Sun and Zhenzhong Chen. 2020. Learned image downscaling for upscaling using content adaptive resampler. *IEEE Transactions on Image Processing (TIP)* 29 (2020), 4027–4040.

Lucas Theis, Wenzhe Shi, Andrew Cunningham, and Ferenc Huszár. 2017. Lossy image compression with compressive autoencoders. In *International Conference on Learning Representations (ICLR)*.

Zhi Tian, Chunhua Shen, and Hao Chen. 2020. Conditional convolutions for instance segmentation. In *European Conference on Computer Vision (ECCV)*.

Longguang Wang, Yingqian Wang, Zaiping Lin, Jungang Yang, Wei An, and Yulan Guo. 2021. Learning A Single Network for Scale-Arbitrary Super-Resolution. In *IEEE/CVF International Conference on Computer Vision (ICCV)*.

Nicolas Weber, Michael Waechter, Sandra C Amend, Stefan Guthe, and Michael Goesele. 2016. Rapid, detail-preserving image downscaling. *ACM Transactions on Graphics (TOG)* 35, 6 (2016), 1–6.

Yue Wu, Guotao Meng, and Qifeng Chen. 2021. Embedding Novel Views in a Single JPEG Image. In *IEEE/CVF International Conference on Computer Vision (ICCV)*.

Menghan Xia, Xueteng Liu, and Tien-Tsin Wong. 2018. Invertible grayscale. *ACM Transactions on Graphics (TOG)* 37, 6 (2018), 1–10.

Mingqing Xiao, Shuxin Zheng, Chang Liu, Yaolong Wang, Di He, Guolin Ke, Jiang Bian, Zhouchen Lin, and Tie-Yan Liu. 2020. Invertible image rescaling. In *European Conference on Computer Vision (ECCV)*.

Yazhou Xing, Zian Qian, and Qifeng Chen. 2021. Invertible image signal processing. In *IEEE/CVF Conference on Computer Vision and Pattern Recognition (CVPR)*.

Brandon Yang, Gabriel Bender, Quoc V Le, and Jiquan Ngiam. 2019. Condconv: Conditionally parameterized convolutions for efficient inference. In *Conference on Neural Information Processing Systems (NeurIPS)*.

Jianchao Yang, John Wright, Thomas S Huang, and Yi Ma. 2010. Image super-resolution via sparse representation. *IEEE Transactions on Image Processing (TIP)* 19, 11 (2010), 2861–2873.

Roman Zeyde, Michael Elad, and Matan Protter. 2010. On single image scale-up using sparse-representations. In *International Conference on Curves and Surfaces*.

Yulun Zhang, Kunpeng Li, Kai Li, Lichen Wang, Bineng Zhong, and Yun Fu. 2018a. Image super-resolution using very deep residual channel attention networks. In *European Conference on Computer Vision (ECCV)*.

Yulun Zhang, Yapeng Tian, Yu Kong, Bineng Zhong, and Yun Fu. 2018b. Residual dense network for image super-resolution. In *IEEE/CVF Conference on Computer Vision and Pattern Recognition (CVPR)*.

Yikang Zhang, Jian Zhang, Qiang Wang, and Zhao Zhong. 2020. Dynet: Dynamic convolution for accelerating convolutional neural networks. *arXiv preprint arXiv:2004.10694* (2020).

Zhisheng Zhong, Tiancheng Shen, Yibo Yang, Zhouchen Lin, and Chao Zhang. 2018. Joint sub-bands learning with clique structures for wavelet domain super-resolution. In *Conference on Neural Information Processing Systems (NeurIPS)*.

Qianshu Zhu, Chu Han, Guoqiang Han, Tien-Tsin Wong, and Shengfeng He. 2020. Video Snapshot: Single Image Motion Expansion via Invertible Motion Embedding. *IEEE Transactions on Pattern Analysis and Machine Intelligence (PAMI)* (2020).